ARTICLE IN PRESS

GEOMOR-03992; No of Pages 11

Geomorphology xxx (2012) xxx–xxx

Contents lists available at SciVerse ScienceDirect

Geomorphology

journal homepage: www.elsevier.com/locate/geomorph

Transient water and sediment storage of the decaying landslide dams induced by the 2008 Wenchuan earthquake, China

Xuanmei Fan [a,b,*], Cees J. van Westen [b], Oliver Korup [c], Tolga Gorum [b], Qiang Xu [a], Fuchu Dai [d], Runqiu Huang [a], Gonghui Wang [e]

[a] The State Key Laboratory of Geohazards Prevention and Geoenvironment Protection (Chengdu University of Technology), Chengdu, Sichuan, China
[b] Faculty of Geo-Information Science and Earth Observation (ITC), University of Twente, 7500 AE, Enschede, P.O. Box 217, The Netherlands
[c] Institute of Earth and Environmental Sciences, University of Potsdam, D-14476 Potsdam, Germany
[d] Institute of Geology and Geophysics, Chinese Academy of Sciences, P.O. Box 9825, Beijing, China
[e] Kyoto University, Disaster Prevention Research Institute, Uji, Kyoto, Japan

ARTICLE INFO

Article history:
Received 17 January 2012
Received in revised form 16 March 2012
Accepted 5 May 2012
Available online xxxx

Keywords:
Landslide dam
Earthquake
Magnitude and frequency
Sediment budget

ABSTRACT

Earthquake-triggered landslide dams are potentially dangerous disrupters of water and sediment flux in mountain rivers, and capable of releasing catastrophic outburst flows to downstream areas. We analyze an inventory of 828 landslide dams in the Longmen Shan mountains, China, triggered by the M_w 7.9 2008 Wenchuan earthquake. This database is unique in that it is the largest of its kind attributable to a single regional-scale triggering event: 501 of the spatially clustered landslides fully blocked rivers, while the remainder only partially obstructed or diverted channels in steep watersheds of the hanging wall of the Yingxiu-Beichuan Fault Zone. The size distributions of the earthquake-triggered landslides, landslide dams, and associated lakes (a) can be modeled by an inverse gamma distribution; (b) show that moderate-size slope failures caused the majority of blockages; and (c) allow a detailed assessment of seismically induced river-blockage effects on regional water and sediment storage. Monte Carlo simulations based on volumetric scaling relationships for soil and bedrock failures respectively indicate that 14% (18%) of the estimated total coseismic landslide volume of 6.4 (14.6) $\times 10^9$ m^3 was contained in landslide dams, representing only 1.4% of the >60,000 slope failures attributed to the earthquake. These dams have created storage capacity of ~0.6×10^9 m^3 for incoming water and sediment. About 25% of the dams containing 2% of the total river-blocking debris volume failed one week after the earthquake; these figures had risen to 60% (~20%), and >90% (>90%) within one month, and one year, respectively, thus also emptying ~92% of the total potential water and sediment storage behind these dams within one year following the earthquake. Currently only ~0.08×10^9 m^3 remain available as natural reservoirs for storing water and sediment, while ~0.19×10^9 m^3, i.e. about a third of the total river-blocking debris volume, has been eroded by rivers. Dam volume and upstream catchment area control to first order the longevity of the barriers, and bivariate domain plots are consistent with the observation that most earthquake-triggered landslide dams were ephemeral. We conclude that the river-blocking portion of coseismic slope failures disproportionately modulates the post-seismic sediment flux in the Longmen Shan on annual to decadal timescales.

1. Introduction

Landslide dams are potentially dangerous obstructions caused by river-blocking slope failures that occur frequently in tectonically active mountains with narrow and steep valleys (Costa and Schuster, 1988). The catastrophic release of water masses from landslide-impounded lakes has produced outburst floods and debris flows, causing loss of lives, housing and infrastructure (Korup, 2002; Dai et al., 2005). Numerous studies have focused on (a) documenting individual catastrophic events and case studies (Hewitt, 1998; Harp and Crone, 2006; Nash et al., 2008; Duman, 2009); (b) evaluating the geomorphic impacts of landslide dams on the fluvial drainage network (Pearce and Watson, 1986; Korup, 2005); (c) qualitatively assessing the stability of landslide dams with geomorphometric and statistical approaches (Ermini and Casagli, 2003; Korup, 2004; Dong et al., 2009); and (d) predicting probable dam-failure modes and the peak discharge of outburst floods (Walder and O'Connor, 1997).

These and other studies emphasized historic case studies, prompting numerous, though often incomplete, compilations of mainly geometric, hydrological, and topographic characteristics (e.g. Casagli and Ermini, 2003; Korup, 2004). Implications of landslide dams induced during

* Corresponding author at: Faculty of Geo-Information Science and Earth Observation (ITC), University of Twente, 7500 AE, Enschede, P.O. Box 217, The Netherlands. Tel.: +31 53 487 4416.
E-mail address: fan21676@itc.nl (X. Fan).

0169-555X/$ – see front matter © 2012 Elsevier B.V. All rights reserved.
doi:10.1016/j.geomorph.2012.05.003

single events such as earthquakes have been rarely studied because of the scarcity of direct observational evidence (Adams, 1981; Pearce and Watson, 1986; Hancox et al., 1997). Here we present one of the first systematic regional studies on the longevity and geomorphic decay of coseismic landslide dams. Derived from detailed remote sensing interpretation and fieldwork, we analyze a unique database of landslide dams triggered by the M_w 7.9 Wenchuan earthquake that struck China's Sichuan Province on 12 May 2008. The earthquake triggered >60,000 landslides (Gorum et al., 2011), out of which >800 formed landslide dams. This database is the largest complete event-based landslide-dam inventory, and provides unprecedented opportunities for studying how natural river blockage modulates the immediate post-earthquake flux of water and sediment at the regional scale. While several earthquakes reportedly caused the formation of hundreds of landslide-dammed lakes (e.g. 1783, Calabria, Italy; Cotecchia and Melidoro, 1974), none of these events has been addressed from the perspective of transient sediment flux tied to the fraction of coseismic slope failures that had blocked rivers. Our objective is to quantitatively constrain the transient sediment budget and residence time of landslide dams following the Wenchuan earthquake. We discuss the implications of their gradual geomorphic decay, which is essential for assessing and mitigating potentially adverse consequences of coseismic river blockage, and its control on post-earthquake sediment flux in the Longmen Shan.

2. Study area

The devastating 2008 (M_w 7.9) Wenchuan, China, earthquake occurred on the NE-trending Longmen Shan thrust fault zone (LTFZ) at a focal depth of 14–19 km. The LTFZ separates the Sichuan basin from the steep and heavily dissected eastern margin of the Tibetan Plateau, with elevations ranging from >5000 m down to 500 m in the Sichuan Basin over a distance of ~50 km. Tributaries of the Yangtze River drain the Longmen Shan as deeply incised bedrock rivers flanked by hillslopes commonly >30° steep within the LTFZ, and underlain by deformed Paleozoic sediments and metamorphic rocks, Mesozoic sediments, and Precambrian crystalline and metamorphic rocks (Kirby et al., 2003).

The LTFZ consists of three sub-parallel faults, i.e. the Wenchuan–Maowen (WMF), Yingxiu–Beichuan (YBF) and Pengguan faults (PF) (Fig. 1). The 2008 rupture initiated near Yingxiu city (31.06° N, 103.33° E), and propagated unilaterally towards the northeast, generating a 240-km long surface rupture along the YBF, and a 72-km long rupture along the PF (Shen et al., 2009; X. Xu et al., 2009). GPS and InSAR data highlight the variability of fault geometry and slip-rate distribution (Hao et al., 2009), showing that in the southwest, from Yingxiu to Beichuan, the fault plane dips moderately to the northwest, as opposed to sub-vertical in the northeast, from Beichuan to the Qingchuan region,

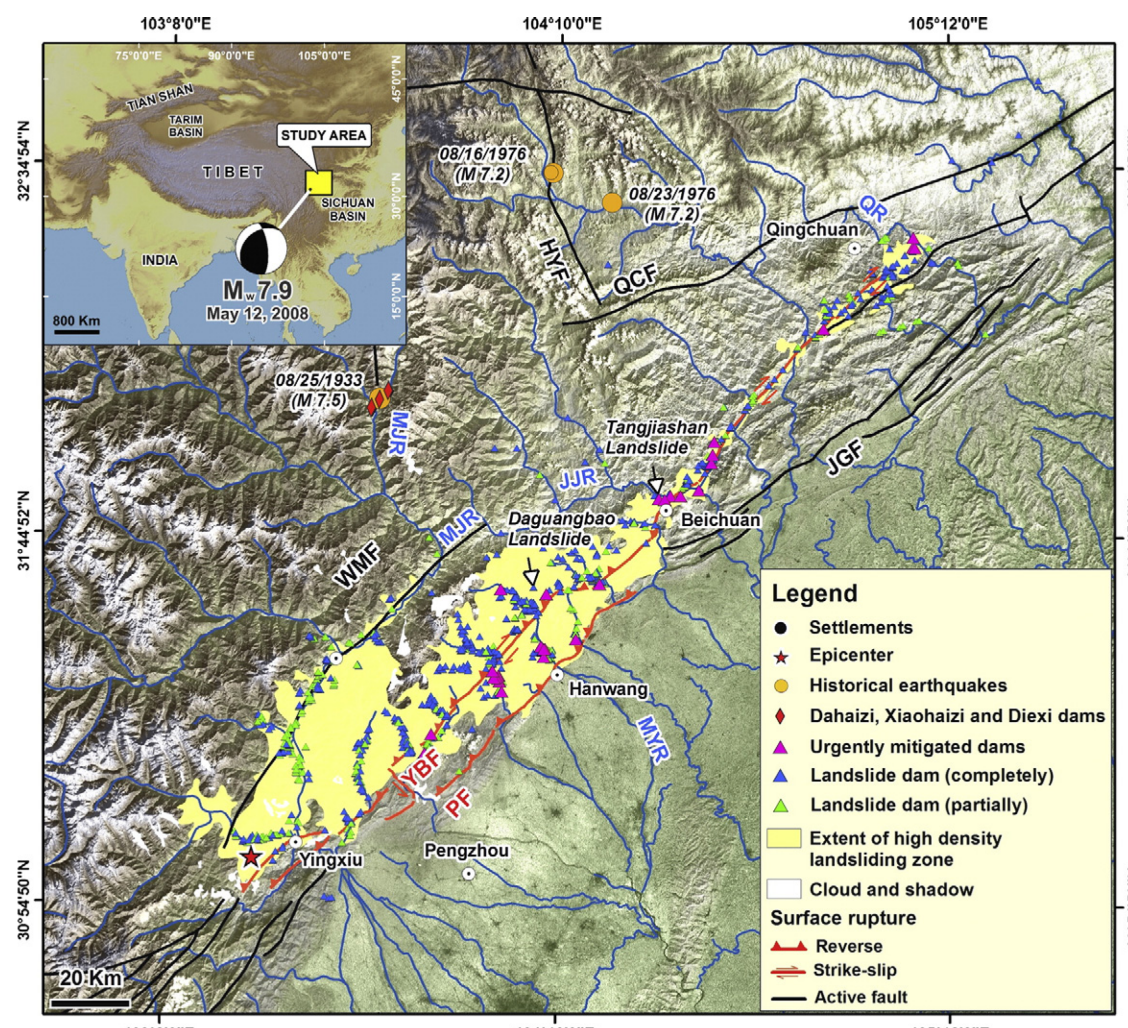

Fig. 1. Distribution of landslide dams triggered by the Wenchuan earthquake, China. The high landslide density zone is defined by a landslide area density >0.1 km^{-2}; also shown are epicenters of historical earthquakes (USGS, 2008) and the historical Diexi landslide dams (Dahaizi, Xiaohaizi and Diexi). White polygons are unmapped due to the presence of clouds and shadows in post-earthquake imagery. WMF: Wenchuan–Maowen fault; YBF: Yingxiu–Beichuan fault; PF: Pengguan fault; JGF: Jiangyou–Guanxian fault; QCF: Qingchuan fault; HYF: Huya fault; MJF: Minjiang fault (after X. Xu et al., 2009). MJR: Minjiang River; MYR: Mianyuan River; JJR: Jianjiang River; QR: Qingjiang River.

Please cite this article as: Fan, X., et al., Transient water and sediment storage of the decaying landslide dams induced by the 2008 Wenchuan earthquake, China, Geomorphology (2012), doi:10.1016/j.geomorph.2012.05.003

associated with a change from predominant thrusting to strike-slip motion. Prior to the Wenchuan earthquake, Li et al. (2008) reported 66 earthquakes with $M_s > 4.7$ mainly concentrated on the Minjiang fault and the southern part of the LTFC since 638 AD, including the M_s 7.5 Diexi earthquake along the Minjiang fault zone in 1933. Two M_s 7.2 earthquakes occurred between Songpan and Pingwu on August 16 and 23, 1976 (Fig. 1). Along the middle and southern part of the LTFZ, three earthquakes were reported in 1657 (M_s 6.5 Wenchuan), 1958 (M_s 6.2 Beichuan), and 1970 (M_s 6.2 Dayi) (Kirby et al., 2000).

Several large earthquake-triggered landslide dams and catastrophic dam-break floods have been documented in the area. On June 1, 1786, an M 7.8 earthquake in the Kangding–Luding area triggered a large ($>10^6$ m^3) landslide dam that blocked the Dadu River. Ten days later, a sudden dam breach caused catastrophic downstream flooding and 100,000 fatalities (Dai et al., 2005). The Diexi earthquake triggered nine large landslide dams on the Min River, three of which (Dahaizi, Xiaohaizi, and Diexi; red diamonds in Fig. 1) were up to 160 m high. The three resulting lakes coalesced seven weeks later, eventually emptying in a dam-break flow that affected a downstream distance of 250 km, killing more than 2,500 people (Chai et al., 2000). The 2008 earthquake highlighted the importance of mitigating the hazards from landslide dams. The Tangjiashan landslide dam had impounded the largest earthquake lake with an estimated volume of 3×10^8 m^3, ~85 km upstream of Mianyang City, i.e. the second largest in Sichuan with a population of 1.2 million. Chinese authorities had to evacuate parts of the city until the Tangjiashan landslide dam had been breached artificially, and the lake was drained (Liu et al., 2009). In order to reduce the potential for further catastrophic dam breaks, the Chinese army created artificial spillways in 32 other dams using explosives and heavy machinery (Q. Xu et al., 2009).

3. Data and methods

Event-based landslide maps record regional patterns of slope failure following single landslide triggering episodes, such as earthquakes or rainstorms, and are essential for generating landslide susceptibility and hazard appraisals (Kamp et al., 2008; Lee et al., 2008; van Westen et al., 2008). Assessments of landslide susceptibility and hazard work on the assumption that inventories of past landslide occurrences are sufficiently representative to predict those in the future. Frequency–area or –volume relationships of landslide inventories are one way of gauging the past abundance, and presumed future probability of landslide occurrence as a function of their size (Stark and Hovius, 2001; Malamud et al., 2004; van den Eeckhaut et al., 2007). To this end, we used the data sources of Gorum et al. (2011), who mapped landslides using 52 pre- and post-earthquake satellite images covering ~35,000 km^2 of the earthquake-affected region. The same data were used in this study, complemented by EO-1 (10 m spatial resolution) of July 2008 and ASTER images (15 m) of July, 2010 for mapping the landslide dams and impounded lakes (see the supplementary material for the spatial coverage of the satellite images and data list). The pre-earthquake images consisted of multispectral data such as ASTER (15 m spatial resolution) and ALOS AVNIR-2 (10 m) as well as panchromatic data from ALOS PRISM (2.5 m) and the Indian Cartosat-1 (2.5 m). Post earthquake images included SPOT-5 (2.5 m), IKONOS (2.5 m), ASTER, ALOS AVNIR-2 and PRISM data as well as aerial photos (0.3 m) which covered most of the large landslides. All aerial photos and satellite images were geometrically corrected using ground-control points (GCPs) measured in the field by Differential GPS and ~200 prominent points selected from 1:50,000-scale digital topographical maps. We used a polynomial nearest neighbor re-sampling method and the GCPs to establish a transformation model for producing the ortho-rectified images with ERDAS Imagine 2010. The geo-rectification accuracy has a root mean square error (RMSE) of <1.5 pixels. We produced a pre-earthquake DEM with 25-m grid spacing from 1:50,000 scale digital topographic maps by interpolating contour lines at intervals of 10 and 20 m for low- and high-relief terrain, respectively. According to the Chinese national standard, the horizontal and vertical accuracy of this 25-m DEM at 90% confidence level is <20 and <10 m, respectively.

We mapped landslide dams through visual interpretation by comparing pre- and post-earthquake false-color composites or panchromatic images, and field checks in accessible areas (Fig. 1). The earthquake-triggered landslides were clearly recognizable from change detection of monoscopic images based on tone, texture, pattern, and shape differences (Fig. 2). Although stereoscopic image interpretation would be better for optimal landslide interpretation, it was practically impossible to generate stereo images for such an extensive area. Therefore, the stereo-based interpretation was only applied to several large landslide dams. Diagnostic features included high reflectance gradients and geomorphic features such as scarps, bare rock-fall talus, and asymmetric hummocky deposits featuring flow lobes, and transverse or longitudinal ridges. Image resolution restricted mapping to landslides and lakes >200 m^2 (footprint area). We classified landslide dams into (a) full blockage, where landslide debris impounded lakes; and (b) partial blockage, where debris obstructed or diverted rivers without forming lakes (Fig. 2a–d). We recorded along-valley dam width, dam height, lake area, and lake volume; as well as planform areas of the river-blocking landslide scars, deposits, and of any associated lakes following definitions by Costa and Schuster (1988) and Korup (2004). Because lake size changes with time due to incoming water and sediment or seepage, we compared multi-temporal images and documented the largest area before any artificial breaching took place. We approximated lake depths and volumes by subtracting the DEM-based pre-earthquake valley-floor elevations from the mapped lake levels at a vertical accuracy of <10 m, assuming that effective dam height corresponded to the mean lake depth at full reservoir capacity. To minimize spurious errors linked to DEM accuracy, we limited our volumetric estimates to 319 lakes with depths >10 m, and areas >1000 m^2. Results were validated using field surveys of 24 lakes conducted by a Chinese expert team and the Chinese army directly after the earthquake (Q. Xu et al., 2009; Fig. 3). Lake volumes were estimated by field measurements of lake area and average lake depth using handheld GPS receivers, laser range finders, and depth soundings from boats (Zhang, 2010).

4. Frequency–size distribution of landslide dams

The landslides triggered by the Wenchuan earthquake affected an estimated overall area of ~811 km^2 (Dai et al., 2011). Fig. 1 shows the distribution of the mapped landslide dams and the full set of coseismic slope failures mapped by Gorum et al. (2011). Bedrock landslides make up 63% of the damming landslides. Our inventory contains 828 river-blocking landslides; 501 (61%) of these fully blocked rivers, while 327 (39%) partially obstructed or diverted channels. While several models have been proposed for describing empirical landslide size–frequency distribution, we find that the three-parameter inverse gamma probability density function used by Malamud et al. (2004), describes sufficiently well the empirical area distributions of all coseismic landslides, landslide dams, and lakes:

$$p(A_L; \rho, a, s) = \frac{1}{a\Gamma(\rho)} \left[\frac{a}{A_L - s}\right]^{\rho+1} \exp\left[-\frac{a}{A_L - s}\right] \quad (1)$$

where A_L is the landslide area; ρ controls the power-law decay for medium and large landslides; a is a location parameter of the maximum probability distribution (m^2); s controls the exponential decay for small landslide areas (m^2); and $\Gamma(\rho)$ is the gamma function of ρ (Malamud et al., 2004). This distribution has a power-law tail with exponent $-(\rho+1)$ for medium and large areas and an exponential rollover for small areas (Fig. 4a, Table 1). Landslide dams have a rollover that is higher by nearly an order of magnitude than that for the entire coseismic landslide sample (14,000 versus 1,500 m^2, respectively; Fig. 4a). Using the fraction of river-blocking landslides out of the

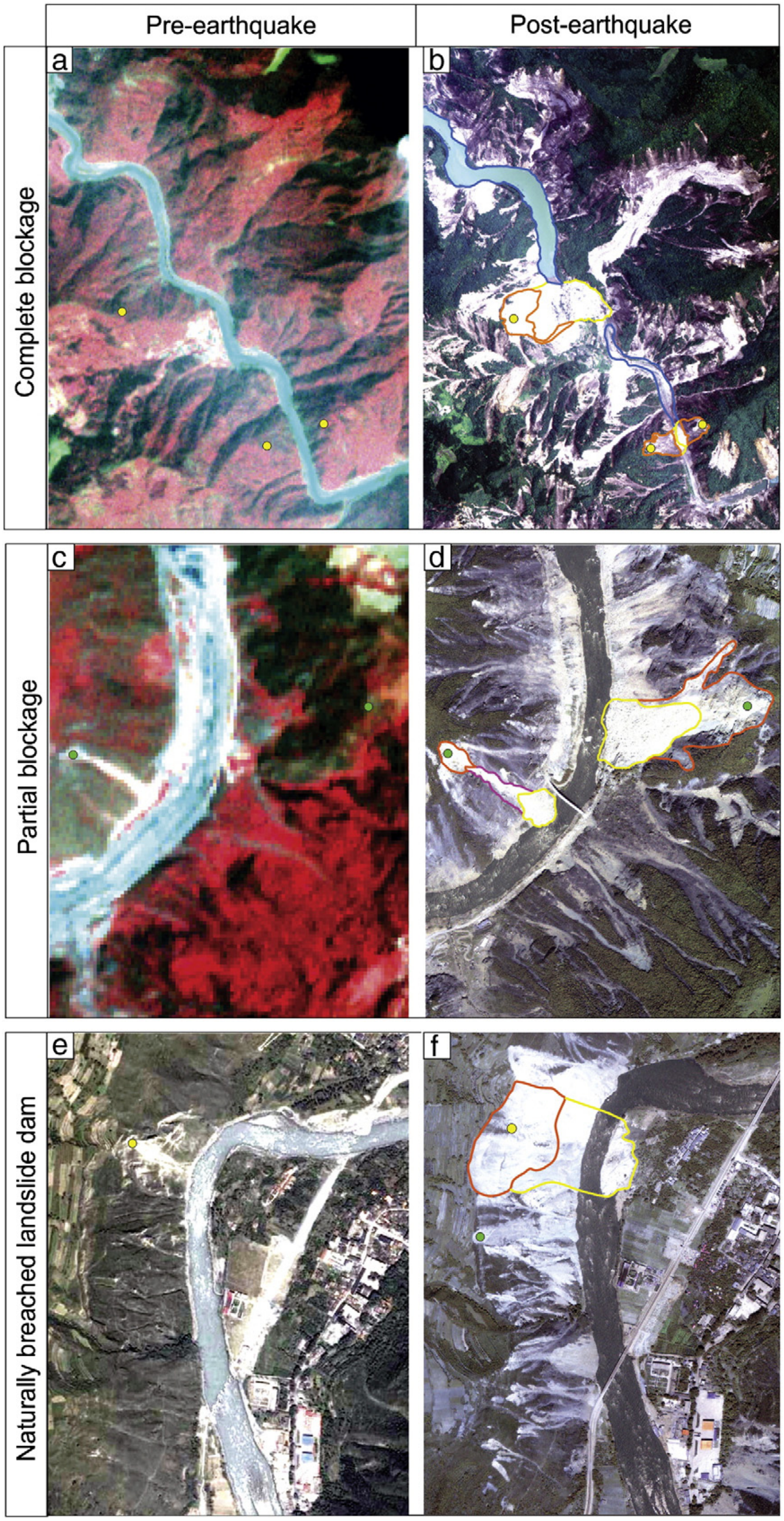

Fig. 2. Examples of completely (a, b) and partially damming landslides (c, d) as observed by comparing pre- and post-earthquake images. Some landslide dams were dissected by rivers already several hours after they were formed (e, f).

landslide number in a given bin to be a proxy of the susceptibility of landslides to form dams, underlines the higher propensity of larger slope failures to interfere with the drainage network (Fig. 4b). Except for the largest event, the Daguangbao landslide (~8×10^8 m^3; Chigira et al., 2010; Huang et al., 2012), deposit volumes of 7–12 $\times 10^6$ m^3 were most prone to impound lakes. Partial dams had areas A_d of 800 m^2 to 1.3 km^2, i.e. spanning more than three orders of magnitude. On average, they were slightly smaller than the fully river-blocking

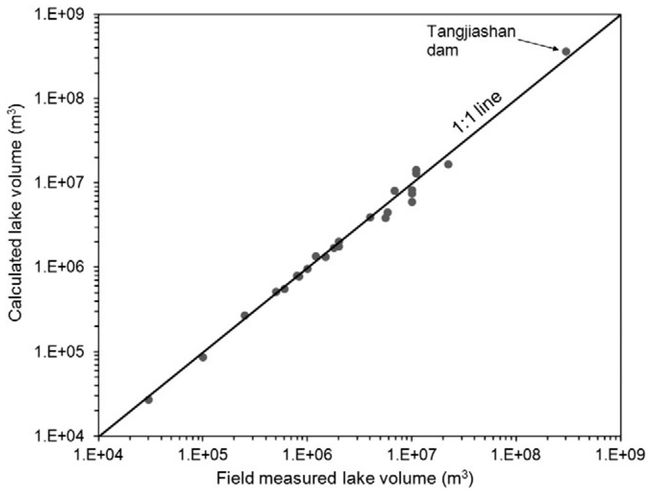

Fig. 3. Validation of the barrier-lake volume estimates using field measurement data.

landslides with A_d of 1,300 m^2 to 7.2 km^2. Overall, some 76 km of river reaches were directly covered by damming landslide debris, exclusive of the reaches affected by backwater inundation by lakes with areas from ~2.0×10^2 to 6.5×10^6 m^2.

5. Geomorphic decay and effects on regional post-seismic sediment flux

The effect of coseismic landslide dams on the overall sediment budget of the earthquake includes the dissected landslide dam materials by fluvial erosion and the backwater storage of sediment transferred from upstream. However, the amount of sediment additionally delivered from backwater sediments is unknown. Therefore, our analysis constrains on analysis of the sediment released from landslide dams through fluvial dissection and their decay. In order to quantify the total mass wasting from the Wenchuan earthquake and their effects on the sediment budget, we expanded the method of Larsen et al. (2010) to constrain the total volume of coseismic landslide debris via a

Table 1
Best fit parameters of the inverse-gamma distributions for the landslide and landslide dam inventories of the Wenchuan earthquake.

Data sets	ρ	a (m^2)	s (m^2)	r^2	Sample number
All landslides	1.11	5.26×10^3	-7.28×10^2	0.85	48006
Partially blocking landslides	2.03	5.56×10^4	-5.00×10^3	0.78	327
Completely blocking landslides	1.40	5.13×10^4	-7.14×10^3	0.89	501
Barrier lakes	0.87	-2.8×10^3	-3.55×10^2	0.86	501

Monte Carlo simulation. Using the mapped landslide (dam) areas (Fig. 4), we estimated each individual landslide volume, V_L:

$$V_L = \alpha A_L{}^{\gamma}, \tag{2}$$

where α is a dimensional coefficient with unit $[A_L^{3-2\gamma}]$ randomly drawn from an interval [0.015; 0.035], and γ is a scaling exponent randomly drawn from an interval [1.1; 1.6] for soil and bedrock landslides, and [1.4; 1.6] for bedrock landslides. Here we use the term “soil” in the engineering geological sense, referring to unconsolidated soil, regolith and colluvium, while "bedrock" refers to a dominance of largely unweathered rock clasts in the landslide mass. We reiterated this estimate for $n=10{,}000$ times for each landslide, and summed up all landslide volumes per sample to obtain probability density estimates of the total volumes (Fig. 5). The parameter intervals are based on published reviews (van den Eeckhaut et al., 2007; Larsen et al., 2010), and designed to allow for maximum variance in terms of environmental boundary conditions for landsliding, and any error sources due to mapping methodology, remote sensing data quality, or statistical derivation of scaling statistics. We used the same method to estimate the potential maximum water and sediment storage in each landslide-dammed lake by using an empirical scaling relationship between lake area and volume that we constrained by field measurements (Fig. 6). We approximated the minimum volume of sediment released from landslide dams through fluvial dissection, V_r, by a simplified geometric relationship

$$V_r = W_d H_d{}^2/\tan\Psi, \tag{3}$$

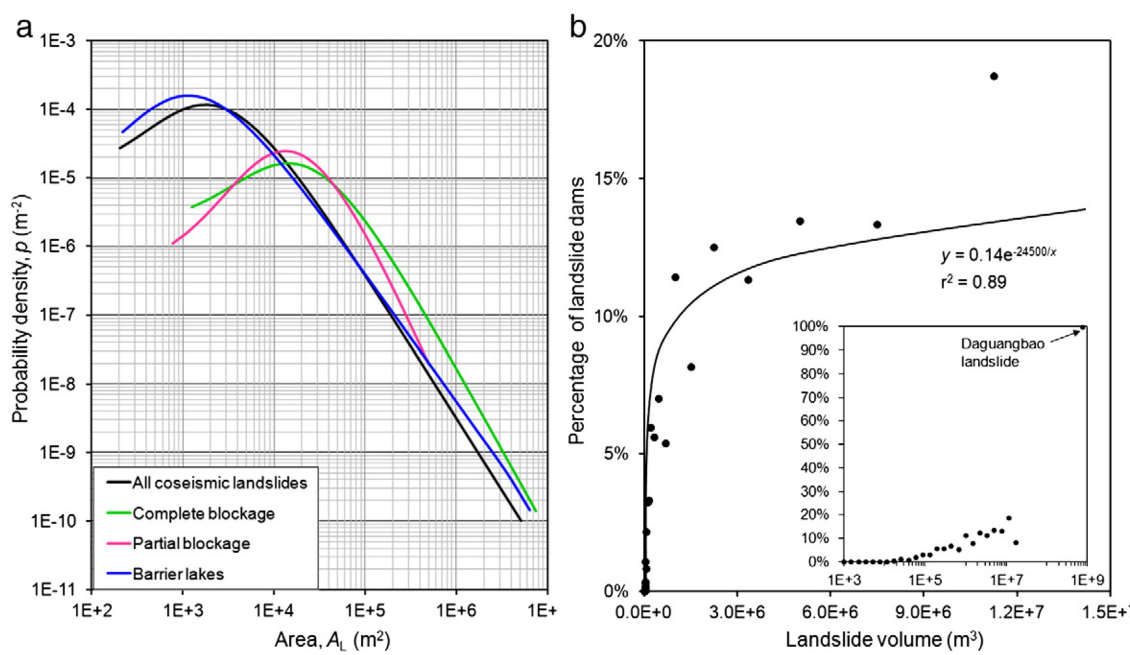

Fig. 4. Probability density analysis and the relationship between landslide volume and percentage of landslide dams. (a) Probability density estimates of all landslides (Dai et al., 2011; Gorum et al., 2011), and those that partially and fully blocked rivers, and the associated barrier lakes (this study); attributed the 2008 Wenchuan earthquake. All data can be modeled with an inverse gamma probability density function (Eq. (1)) that we fitted using a maximum-likelihood estimator. (b) Landslide volume versus percentage of landslide dams. Note how the peak density of river-blocking landslides is one order of magnitude higher compared to the peak density of all coseismic landslides.

Please cite this article as: Fan, X., et al., Transient water and sediment storage of the decaying landslide dams induced by the 2008 Wenchuan earthquake, China, Geomorphology (2012), doi:10.1016/j.geomorph.2012.05.003

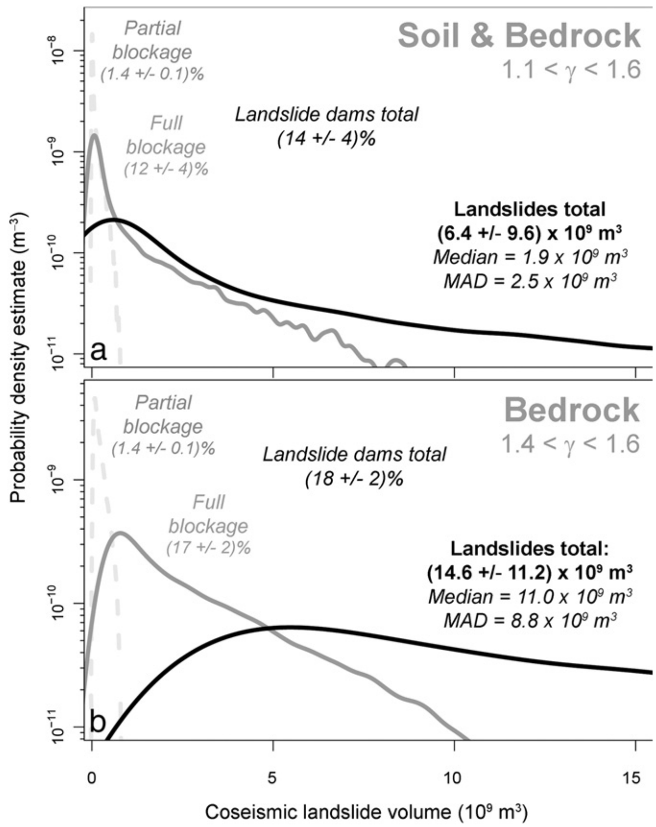

Fig. 5. Probability density estimates of total volumes of coseismic landslides (black lines), including those having caused full, and partial river blockage (light and dark gray lines, respectively) triggered by the 2008 Wenchuan earthquake. Percentages are a fraction of the total volumetric estimate. Volumes for each landslide were derived by $n = 10{,}000$ random draws of scaling parameters in Eq. (2) from fixed intervals, before being summed up for total volumes, for (a) both soil and bedrock landslides; and (b) mainly bedrock landslides. γ is a scaling exponent of the volume–area power-law relationship. *MAD* = median absolute deviation.

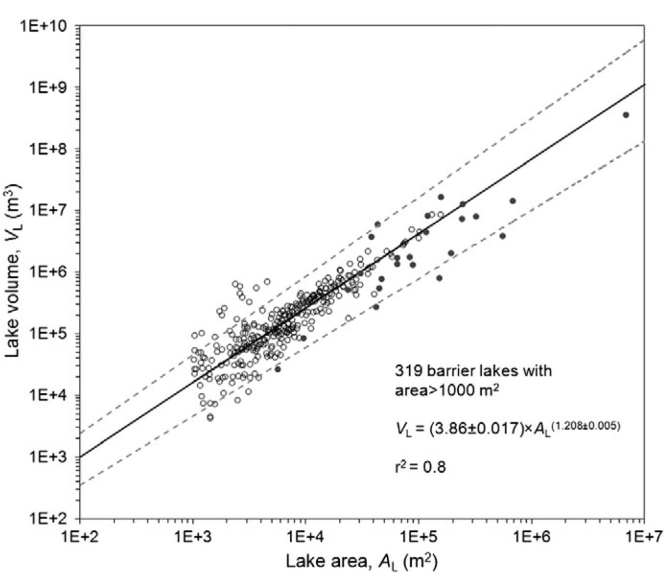

Fig. 6. Empirical scaling relationship between landslide-dammed lake volume V_L and area A_L. Filled circles represent lakes with field measured volume as shown in Fig. 2. Thick black line is best fit obtained by the Reduced Major Axis Regression (RMA). Dashed grey lines show 95% confidence intervals. We used this relationship to estimate the regional storage capacity for water and sediment behind landslide dams.

where W_d is the along-valley width of the landslide dam, H_d is the average dam height, and Ψ is the mean bank angle of the breach channel cut through the dam. This approximation assumes a straight, symmetrically v-shaped breach channel of negligible gradient in uniform material with Ψ being 32° to 37°, and reproduces the central tendency of a global dataset of dissected landslide dams (Fig. 7).

Our Monte Carlo based estimates of the mean total coseismic landslide debris are $(6.4 \pm 9.6) \times 10^9$ or $(14.6 \pm 11.2) \times 10^9$ m^3, depending on whether we use volumetric scaling parameters for soil or mixed soil and bedrock landslides, respectively (Fig. 5; Larsen et al., 2010). While the river-blocking landslides make up only 1.4% of the total coseismic landslide number, their volumetric fraction is 14% and 18%, respectively.

Some landslide dams, particularly those caused only partial obstruction, were dissected by rivers already several hours after they were formed (Fig. 2e, f). We define a failure rate as the volumetric fraction of landslide dams that failed in time intervals bracketed by multi-temporal satellite imagery (Table 2; Fig. 8). ASTER scenes of July 2010 show that 5% of the fully river-blocking landslides remained intact 26 months after the earthquake. These 23 landslide dams accounted for around 45% of the total landslide dam volume, and were mainly formed by complex deep-seated slope failures (Table 2). Since these survival dams are either located in remote regions or impounded very small lakes along tributaries, no attempts have been done to breach these dams artificially. Altogether, some 60% of dams, constituting 20% of the total landslide-dam volume, failed within one month after the earthquake (Table 2; Fig. 8). This rapid decrease leveled off two months after the earthquake. The earthquake occurred during the rainfall season, therefore most of the small landslide dams would have filled up quickly and failed by overtopping. Heavy rainstorms could have also been a major cause of the failure of ~90% dams within one year after the earthquake. One storm occurred four months after the earthquake, (Sep 24, 2008), causing not only the breach of several dams but also triggering 72 debris flows in the epicenter region (Tang et al., 2009). Also, the failure of large dams upstream may cause the cascading breach of the smaller downstream dams. For example, the artificial breach of the Tangjiashan landslide dam resulted in the failure of five smaller dams downstream.

The total volumes of both landslide dams and lakes estimated from Eq. (2) show a similar nonlinear decay with time. Altogether, a reservoir volume of $> 0.57 \times 10^9$ m^3 formed behind 319 of the 828 landslide dams. About two third of this temporary storage capacity for incoming water and sediment had been associated with the Tangjiashan landslide dam, and its artificial breaching on June 10, 2008 stands out as a conspicuous bump in the volumetric decay curve. From Eq. (3) we estimate that the volume of sediment liberated by dissection of landslide dams is $(0.19 \pm 0.01) \times 10^9$ m^3, i.e. <5% of the total volume mobilized by coseismic landslides (Fig. 8b).

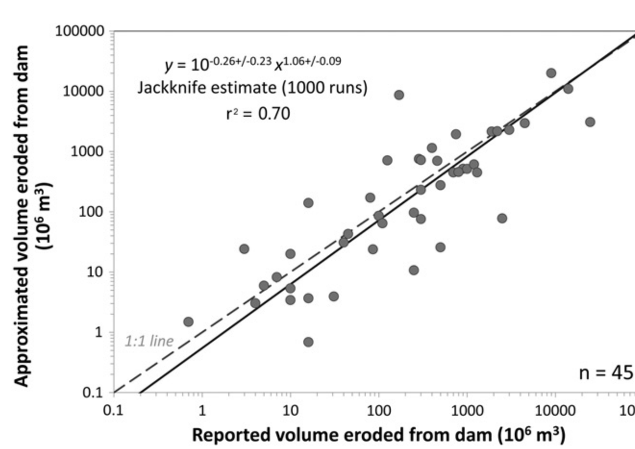

Fig. 7. Approximation of the volume of dissected landslide dams from a global date set.

Table 2
Summary of multi-temporal remote sensing data used for assessing the landslide dam decay (failure) rate.

Data covered region	Date	Sensor	Resolution (m)	Barrier lake and landslide dam decay rate		
				Percent of dam number (%)	Percent of lake volume (%)	Percent of dissected dam volume (%)
Around Beichuan area, including 65 landslide dams	May 18, 2008	ALOS PRISM/Aerial photos	2.5/0.3	24.6	1.0	2.0
	Oct 13, 2008	SPOT-5	2.5	93.8	91.0	95.8
	Jan 24, 2009	CARTOSAT-1	2.5	95.4	92.0	96.0
	July 19, 2010	ASTER	15	95.4	92.0	96.0
Pengzhou area, including 77 landslide dams	June 4, 2008	ALOS AVNIR-2	10	57.1	13.7	15.6
	July 8, 2008	EO-1	10	76.6	77.1	22.3

6. Spatial distribution of landslide dams and morphometric controls on dam stability

6.1. Spatial distribution of landslide dams

For a comparison of the spatial pattern of landslides and landslide dams we decided to use the point information generated by Gorum et al. (2011), rather than the polygon data from Dai et al. (2011) as the latter one did not cover the entire area. We estimated the spatial density of all coseismic landslides, and landslide dams, within a circular moving window of 1-km radius, obtaining maximum density values of 54.1 km^{-2}, and 4.5 km^{-2}, respectively (Fig. 9a, b). A 240-km by 25-km rectangular swath profile along the LTFZ illustrates variations in spatial abundance of (river-blocking) landslides (Fig. 9c). The 25 km width of the swath profile region was selected to represent the extent of the surface projection of the hanging wall of the Yingxiu–Beichuan fault. The landslide-dam abundance peaks near the drainage network, spatially mimicking the pattern of coseismic landslide abundance (Fig. 9c). Landslide and landslide-dam densities on the hanging wall of the Yingxiu–Beichuan fault (YBF) generally exceed those on the footwall. Landslide dams are most abundant in steep watersheds (P1–P7) of the Pengguan Massif, along the thrust segment of the Yingxiu–Beichuan fault (YBF, Fig. 9b). Their density decreases dramatically to the NE, extending from Beichuan Town to the fault tip. The Pengguan Massif is composed of fragmented Precambrian crystalline gneisses and granites separated from a series of Triassic mudstones by the YBF. Apart from lithologic and seismic controls on landslide (dam) distribution, fluvial erosion potential also plays an important role, which is commonly inferred from a power-law relationship between river-bed slope S and upstream drainage area A_c,

$$S = k_s A_c^{-\theta}, \tag{4}$$

where k_s is the channel steepness index, and θ is the concavity index (e.g. Whipple, 2004). Assuming that k_s carries vital information about fluvial erosion potential (e.g. Kirby et al., 2003), we computed the normalized steepness for fully and partially dammed river segments, using a fixed $\theta = 0.45$, a value common to rivers in active mountain belts (Whipple, 2004). We find that the Min River catchment (MJR), and catchments in the Pengguan Massif (P1-P7) have by far the highest k_s values, reflecting high-relief bedrock gorges flanked by steep hillslopes promoting landslide (dam) occurrence: More than 75% of landslide dams concentrated there, and >90% of the landslides along the MJR formed partial dams (Fig. 10).

6.2. Morphometric controls on landslide-dam stability

The stability of landslide dams is a function of their geometry, internal structure, material properties, lake volume, inflow rate, and seepage processes (Costa and Schuster, 1988). Unfortunately, the internal structure and particle size distribution become evident only after dam failure such that reliably predicting landslide-dam stability remains a key challenge. Casagli and Ermini (2003) showed that geomorphometric parameters help assess to first order the state of stability of landslide dams, rather than their geotechnical stability. They proposed a blockage index (I_b):

$$I_b = \log\left(\frac{V_D}{A_C}\right) \tag{5}$$

where V_D is the volume of the landslide dam [m^3], and A_C is the catchment area upstream of the dam [km^2]. We plotted I_b for the 23 existing lakes behind currently intact landslide dams, those that had been breached in different catchments, and those that were mitigated by authorities (Fig. 10b). We observe that no full blockages or lakes formed where I_b<2, whereas dams had breached where I_b<4, including some

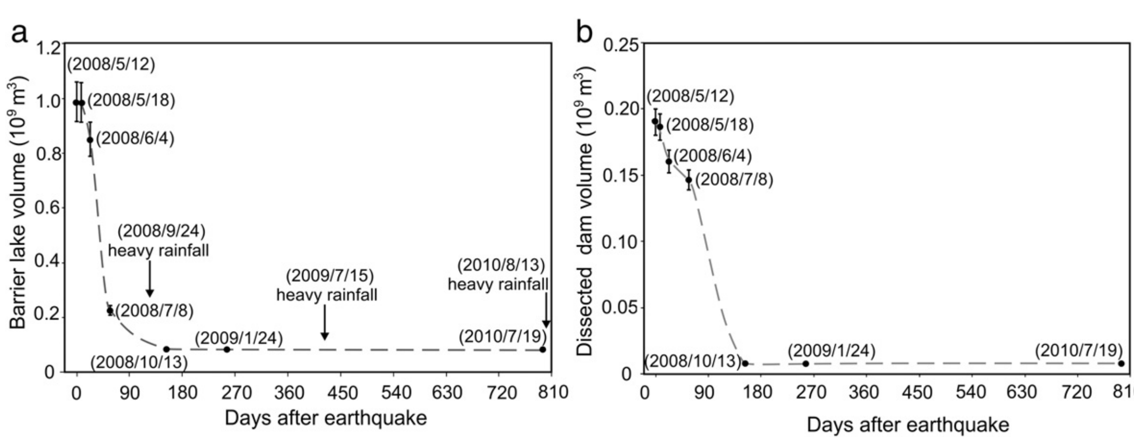

Fig. 8. Time series of loss of volume of (a) estimated water and storage in landslide-dammed lakes, and (b) dissected landslide dams through breaching and subsequent fluvial erosion. Note that this is an overestimate given that parts of the dams may remain in place. Error bars show ±1 s.d. error.

Please cite this article as: Fan, X., et al., Transient water and sediment storage of the decaying landslide dams induced by the 2008 Wenchuan earthquake, China, Geomorphology (2012), doi:10.1016/j.geomorph.2012.05.003

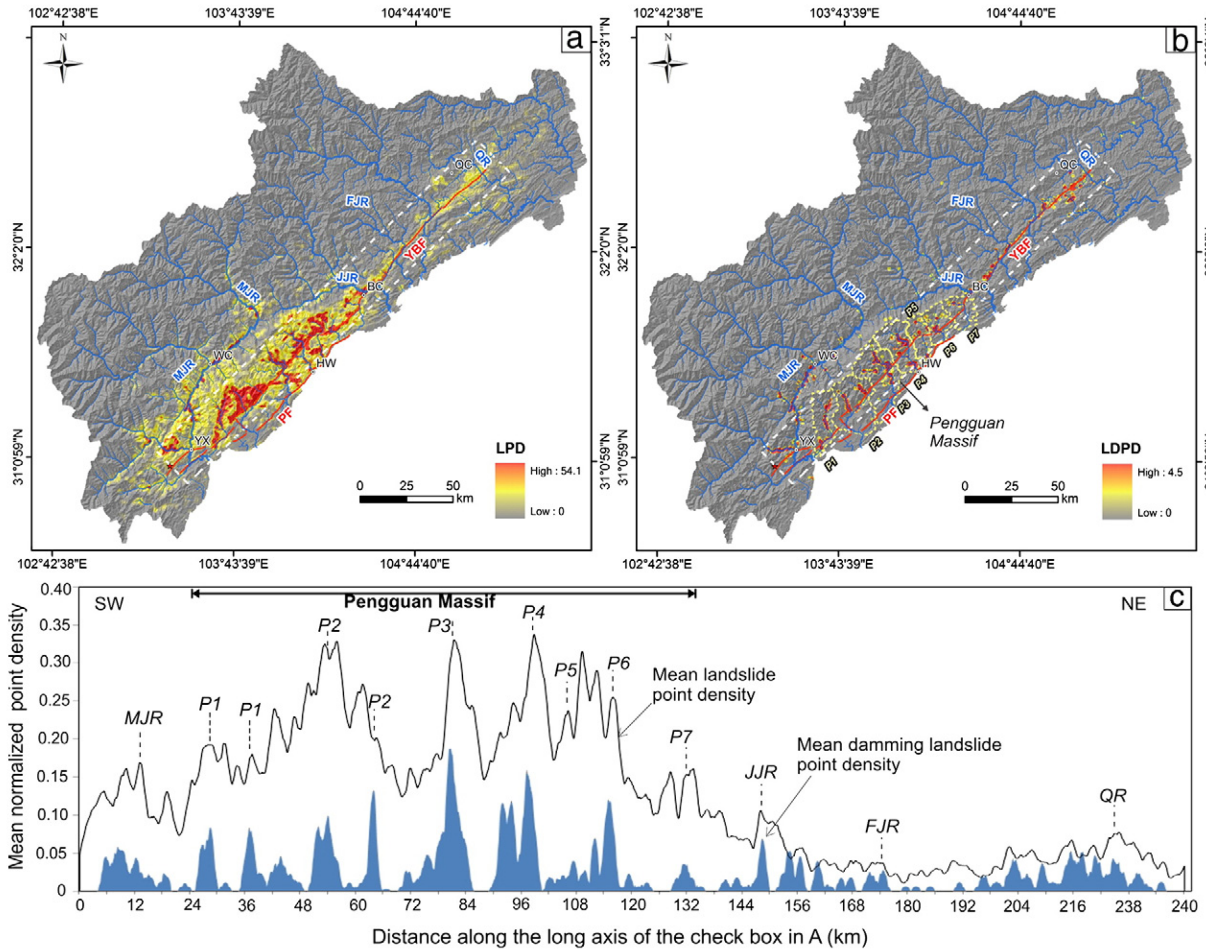

Fig. 9. Comparison of densities of blocking and non-blocking landslides. (a) Landslide density. (b) Landslide dam point density. White dashed lines are 240-km by 25-km swath profiles. (c). Mean normalized landslide and landslide dam densities along the SW–NE profile. Red lines are Yingxiu-Beichuan fault (YBF) and Pengguan fault (PF). Yellow dash lines are the boundary of the P1–P7 watersheds in the Pengguan Massif. YX, WC, HW, BC, and QC are the cities of Yingxiu, Wenchuan, Hanwang, Beichuan and Qingchuan, respectively. MJR, JJR, FJR, and QR represent Minjiang, Jianjiang, Fujiang and Qingjiang rivers, respectively.

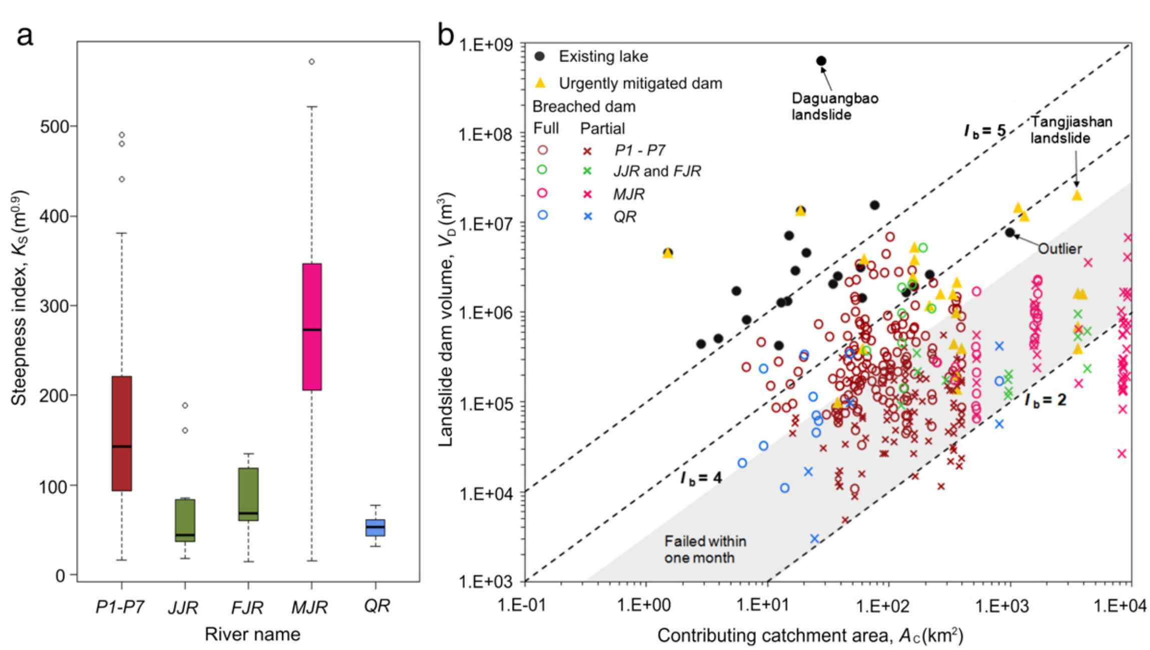

Fig. 10. Steepness and blockage index plots. (a) Boxplot of the steepness index of fully and partially dammed river segments in different catchments. (b) Contributing catchment area versus landslide dam volume for 501 coseismic landslide dams with empirical envelope curves for the blockage index I_b. Most of landslide dams in the grey shaded domain failed within one month after the earthquake. P1–P7, MJR, JJR, FJR and QR are the watersheds and rivers in the study area as shown in Fig. 9.

75% of the artificially breached dams. Most of landslide dams in the gray shaded domain in Fig. 10b failed within one month after the earthquake. Barrier lakes where $I_b > 5$ have remained intact revealed by the July 2010 ASTER images. We also find that the state of stability varies with k_s. Only ~4% of the complete dams remained intact in the P1–P7 catchments, and none in the MJR with the highest k_s, while ~15% of dams in JJR, FJR and QR catchments, where k_s is lower, remained intact.

7. Discussion

Our inventory of landslide dams caused by the Wenchuan earthquake is unique in that it records abundant river blockage following a single regional landslide triggering event. We used this inventory to focus on immediate, i.e. annual-scale post-earthquake dynamics of landslide dams at the regional scale, assessing the decay of dam intactness and its influence on the post-seismic sediment flux. Our volumetric estimates were designed to quantify regional-scale sediment generation through landsliding and sediment delivery from the fluvial dissection of landslide dams. These estimates rely on a number of assumptions and simplifications, including (1) empirical volume–area scaling for both landslides and landslide-dammed lakes; (2) a maximum effective landslide (dam) mapping resolution in space and time dictated by the remote sensing data quality; and (3) geometric simplifications adhering to the estimates of how much sediment was eventually removed from breached or dissected landslide dams.

With regard to (1), our volumetric estimates corroborate those by Parker et al. (2011), who suggested that earthquake-triggered landslides involved $5–15\times10^9$ m^3. While our estimates overlap with this range (Fig. 4), the obvious deviations highlight the importance of using statistically robust methods for approximating mass balances related to regional slope-failure episodes. Our Monte Carlo approach to estimating the total coseismic volume has the advantage that it (a) does not rely on a single volumetric scaling relationship; (b) helps include constraints set by landslide type and material (Larsen et al., 2010); and (c) allows quantifying the inherent error margins as well as their propagation based on a large number ($n = 10{,}000$) of permutations in the scaling parameters. The percentage of river-blocking landslides in terms of volume remains at 14–18%, and demonstrates that a significant fraction of landslides has the potential to interfere with the flow of water and sediment in the drainage network.

Concerning (2), other error sources such as cloud cover or shadow effects are inherent to the remote sensing based mapping approach. Together with the time lag between earthquake and image capture, these preclude the compilation of landslide-dam complete inventories. Optical data are of limited use especially where multiple indistinguishable landslides have stripped hillslopes bare of any vegetation cover. Such pervasive stripping of vegetation cover at the scale of individual hillslopes may bias landslide mapping towards a higher abundance of larger landslides at the expense of smaller slope failures with contiguous or ill-defined scars, thus potentially favoring higher landslide volumetric estimates.

Regarding (3), the approach of evaluating the amount of sediment removed from the landslide dams is simple, but seems to capture to first order the overall trend of the sediment flux following dam failures, given that field observations confirm that in most cases only minor fractions of the river-blocking material has been sluiced downstream. However, while the geomorphic decay of landslide dams supports earlier reported trends of the rather short-lived nature of most of these blockages, their removal by fluvial erosion is slower. On valley floors, the formation of >800 landslide dams had created a temporary sediment storage consisting of dams and backwater, i.e. lacustrine and fluvial deposits with a volume corresponding to 20–25% of that mobilized during the earthquake on hillslopes. Yet most of this potential storage was obliterated and removed within several years following the earthquake.

Despite these caveats our results underline that river-blocking landslides involve disproportionate fractions of the total coseismic mass balance. While the spatial distribution of landslide dams mimics that of the coseismic landslides, particularly steep and high-relief bedrock gorges promote not only spatially clustered but also short-lived (<1 year) natural river blockage. The rapid geomorphic decay of the mapped landslide dams supports earlier observations on selected worldwide data (Costa and Schuster, 1988). Our results also indicate that the normalized channel steepness index may be a useful measure for predicting the longevity of landslide dams, though further research is needed to test this notion. While fluvial dissection and artificial draining of a number of dams has contributed to emptying >90% of the potential backwater storage volumes, significant amounts of formerly river-blocking debris remains on valley floors and awaits entrainment during sufficiently competent floods. Hence, while the immediate hazard of catastrophic lake outbursts has been largely mitigated, we anticipate that significant sediment pollution may continue to be a major problem for rivers in the earthquake-affected region and their downstream reaches.

Our results also contribute to improving our understanding of how large earthquakes serve to build mountains through uplift, while also reducing local topography through widespread coseismic landsliding. Parker et al. (2011) estimated that the total volume of coseismic landslides triggered by the Wenchuan earthquake exceeded the volume of material added to the orogen through rock uplift, concluding that the earthquake caused a net loss in topography. Critical to this assessment is the fraction of landslide debris that is exported from the earthquake-affected region by fluvial erosion before the next similar disturbance takes place (Yanites et al., 2010; Hovius et al., 2011). Our analysis of volume decay of dissected landslide dams captures the short-term dynamics of sediment transport (Fig. 8b), and shows that 0.19×10^9 m^3, i.e. only <5% of the total coseismic landslide volume, has been carried away within two years after the earthquake, leaving 82–86% still suspended on hillslopes, and 9–13% stored close to the drainage network as intact or formerly river-blocking deposits. Thus, the volume of landslide materials being removed by rivers so far is about 5–13% of the inferred volume gained from tectonic uplift, i.e. 2.6 ± 1.2 km^3 (Parker et al., 2011). Debris-flow episodes triggered by the three large post-earthquake rainstorms (Tang et al., 2009) remobilized and delivered only a very small fraction (~0.01×10^9 m^3) of the loose earthquake-derived debris from hillslopes to channels. Part of this low sediment delivery ratio to rivers may be due to the observation that most of earthquake-induce landslides initiate from the upper part of slopes or mountain ranges, and terminate on mid-slope portions (Meunier et al., 2008). The lack of pre- and post- earthquake sediment discharge data together with extensive disaster intervention and reconstruction efforts in many of the Longmen Shan's valleys precludes more accurate assessments of the post-earthquake sediment flux. The experience from 1999 Chi-Chi earthquake, Taiwan, (Lin et al., 2008; Hovius et al., 2011) showed that earthquake effects of enhancing fluvial suspended sediment loads dissipated some six years after the earthquake. Given that the less steep and less typhoon-drenched rivers of the Longmen Shan were affected by a much higher amount of river-blocking landslides, higher landslide numbers, and overall sediment input, we anticipate that the post-seismic sedimentary effects of the Wenchuan earthquake wear off more slowly than in the Taiwan case. Based on the distribution of I_b values of the landslide-dam data, we speculate that the 23 survival landslide dams containing 45% of the coseismic landslide dams in volume, or 6% of the total coseismic landslide debris volume, may remain intact for an unspecified period of time, thus trapping further water and sediment. Eventually, however, the competition between uplift and erosion on timescales integrating multiples of the recurrence intervals of such large earthquakes will determine whether events such as the Wenchuan earthquake cause net build-up or net decay of mountain topography (Ouimet, 2010). The recurrence interval of this earthquake magnitude is estimated at 2000–4000 year (Shen et al., 2009; Ran et al., 2010), and crucial for estimating the size–frequency distribution of landslides and landslide dams triggered by the next event.

8. Conclusions

The 2008 Wenchuan earthquake provided a unique opportunity to study an event-based landslide dam inventory of 828 coseismic landslide dams, and 501 associated lakes. This rare occasion provides insights on the spatio-temporal clustering and geomorphic decay of coseismic landslide dams. In summary, the formation and failure of landslide dams has involved significant fractions (14–18%) of the overall volumetric sediment generation of the 2008 Wenchuan earthquake, though recruiting only 1.4%, and mostly the larger, of all slope failures as temporary sediment storage on the valley-floor. Backwater impoundments constituted an estimated 20–25% of the total volume of material moved, but were gradually reduced during natural and artificial dam breaches. The volume of sediment released to trunk rivers is estimated at 0.19×10^9 m^3, i.e. <5% of the total coseismic landslide volume, and mainly occurred within a couple of years after the earthquake and future impacts are anticipated to occur on annual timescales. In essence, about only a third of the sediment volumes contained in landslide dams has been flushed downstream. However, the remaining landslide-dam debris together with that of the bulk volume (>85%) of smaller landslides await flushing during major sediment pulses in years and decades to come. On annual to decadal time scales, these findings have important implications for future flood and sediment management of the river systems in the earthquake-affected areas, given that many settlements have been re-established near active floodplains of major trunk rivers. On longer timescales, seismic and post-seismic sediment budgets will help quantitatively resolve the topographic net effect of large earthquakes that culminate in the competition between mountain-belt formation through uplift, and topographic decay through coseismic landsliding.

Acknowledgements

This research was financially supported by the National Natural Science Foundation of the People's Republic of China (41130745), in collaboration with the United Nations University – ITC School for Disaster Geo-Information Management, University of Twente, The Netherlands. O. Korup acknowledges support by the German Research Foundation (Heisenberg Program). Helpful comments by David Alexander, Niels Hovius, and several anonymous reviewers improved earlier drafts. We thank Dr. Yijian Zeng, ITC, for his support on the size–frequency analysis, and the Japan Aerospace Exploration Agency (JAXA), GeoEye foundation, and Indian Space Research Organisation (ISRO) for providing data.

Appendix A. Supplementary data

Supplementary data to this article can be found online at http://dx.doi.org/10.1016/j.geomorph.2012.05.003.

References

Adams, J., 1981. Earthquake-dammed lakes in New Zealand. Geological Society of America, Geology 9, 215–219.
Casagli, N., Ermini, L., 2003. Determining grain size distribution of the material composing landslide dams in the Northern Apennines: sampling and processing methods. Engineering Geology 69, 83–97.
Chai, H., Liu, H., Zhang, Z., Xu, Z., 2000. The distribution, causes and effects of damming landslides in China. Journal of the Chengdu Institute of Technology 27, 302–307.
Chigira, M., Xu, X., Inokuchi, T., Wang, G., 2010. Landslides induced by the 2008 Wenchuan earthquake, Sichuan, China. Geomorphology 118, 225–238.
Costa, J.E., Schuster, R.L., 1988. The formation and failure of natural dams. Geological Society of America Bulletin 100, 1054–1068.
Cotecchia, V., Melidoro, G., 1974. Some principal geological aspects of the landslides of Southern Italy. Bulletin of Engineering Geology and the Environment 9, 23–32.
Dai, F., Lee, C.F., Deng, J., Tham, L.G., 2005. The 1786 earthquake-triggered landslide dam and subsequent dam-break flood on the Dadu River, southwestern China. Geomorphology 65, 205–221.
Dai, F., Xu, C., Yao, X., Xu, L., Tu, X., Gong, Q., 2011. Spatial distribution of landslides triggered by the 2008 Ms 8.0 Wenchuan earthquake, China. Journal of Asian Earth Sciences 40, 883–895.
Dong, J., Tung, Y.H., Chen, C.C., Liao, J., Pan, Y., 2009. Discriminant analysis of the geomorphic characteristics and stability of landslide dams. Geomorphology 110, 162–171.
Duman, T.Y., 2009. The largest landslide dam in Turkey: Tortum landslide. Engineering Geology 104, 66–79.
Ermini, L., Casagli, N., 2003. Prediction of the behavior of landslide dams using a geomorphological dimensionless index. Earth Surface Processes and Landforms 28, 31–47.
Gorum, T., Fan, X., van Westen, C.J., Huang, R., Xu, Q., Tang, C., Wang, G., 2011. Distribution Pattern of Earthquake-induced Landslides Triggered by the 12 May 2008 Wenchuan Earthquake. Geomorphology 133, 152–167.
Hancox, G.T., Perrin, N.D., Dellow, G.D., 1997. Earthquake-induced landsliding in New Zealand and implications for MM intensity and seismic hazard assessment. Client Report 43601B prepared for Earthquake Commission Research Foundation. Institute of Geological and Nuclear Sciences, Lower Hutt. 85 pp.
Hao, K.X., Si, H., Fujiwara, H., Ozawa, T., 2009. Coseismic surface-ruptures and crustal deformations of the 2008 Wenchuan earthquake Mw 7.9, China. Geophysical Research Letters 36, L11303, http://dx.doi.org/10.1029/2009GL037971.
Harp, E.L., Crone, A.J., 2006. Landslides Triggered by the October 8, 2005, Pakistan Earthquake and Associated Landslide-Dammed Reservoirs. U.S. Geological Survey Open-file Report 2006–1052. 13 pp.
Hewitt, K., 1998. Catastrophic landslides and their effects on the Upper Indus streams, Karakoram Himalaya, northern Pakistan. Geomorphology 26, 47–80.
Hovius, N., Meunier, P., Lin, C., Chen, H., Chen, Y., Dadson, S., Horng, M.J., Lines, M., 2011. Prolonged seismically induced erosion and the mass balance of a large earthquake. Earth and Planetary Science Letters 304, 347–355.
Huang, R., Pei, X., Fan, X., Zhang, W., Li, S., Li, B., 2012. The characteristics and failure mechanism of the largest landslide triggered by the Wenchuan earthquake, May 12, 2008, China. Landslides 9, 131–142.
Kamp, U., Growley, B.J., Khattak, G.A., Owen, L.A., 2008. GIS-based landslide susceptibility mapping for the 2005 Kashmir earthquake region. Geomorphology 101, 631–642.
Kirby, E., Whipple, K.X., Burchfiel, B.C., Tang, W., Berger, G., Sun, Z., Chen, Z., 2000. Neotectonics of the Min Shan, China: implications for mechanisms driving Quaternary deformation along the eastern margin of the Tibetan Plateau. Geological Society of America Bulletin 112, 375–393.
Kirby, E., Whipple, K.X., Tang, W., Chen, Z., 2003. Distribution of active rock uplift along the eastern margin of Tibetan Plateau: Inferences from bedrock channel longitudinal profiles. Journal of Geophysical Research 108, 1–24.
Korup, O., 2002. Recent research on landslide dams-a literature review with special attention to New Zealand. Progress in Physical Geography 26, 206–235.
Korup, O., 2004. Geomorphometric characteristics of New Zealand landslide dams. Engineering Geology 73, 13–35.
Korup, O., 2005. Geomorphic imprint of landslides on alpine river systems, southwest New Zealand. Earth Surface Processes and Landforms 30, 783–800.
Larsen, I.J., Montgomery, D.R., Korup, O., 2010. Landslide erosion controlled by hillslope material. Nature Geoscience 3, 247–251.
Lee, C.T., Huang, C.C., Lee, J.F., Pan, K.L., Lin, M.L., Dong, J.J., 2008. Statistical approach to earthquake-induced landslide susceptibility. Engineering Geology 100, 43–58.
Li, X., Zhou, Z., Yu, H., Wen, R., Huang, M., Zhou, Y., Cu, J., 2008. Strong motion observations and recordings from the great Wenchuan Earthquake. Earthquake Engineering and Engineering Vibration 7, 235–246.
Lin, G., Chen, H., Hovius, N., Horng, M.J., Dadson, S., Meunier, P., Lines, M., 2008. Effects of earthquake and cyclone sequencing on landsliding and fluvial sediment transfer in a mountain catchment. Earth Surface Processes and Landforms 33, 1354–1373.
Liu, N., Zhang, J., Lin, W., Cheng, W., Chen, Z., 2009. Draining Tangjiashan Barrier Lake after Wenchuan Earthquake and the flood propagation after the dam break. Science in China Series E: Technological Sciences 52, 801–809.
Malamud, B.D., Turcotte, D.L., Guzzetti, F., Reichenbach, P., 2004. Landslides, earthquakes, and erosion. Earth and Planetary Science Letters 229, 45–59.
Meunier, P., Hovius, N., Haines, A.J., 2008. Topographic site effects and the location of earthquake induced landslides. Earth and Planetary Science Letters 275, 221–232.
Nash, T., Bell, D., Davies, T., Nathan, S., 2008. Analysis of the formation and failure of Ram Creek landslide dam, South Island, New Zealand. New Zealand Journal of Geology and Geophysics 51, 187–193.
Ouimet, W.B., 2010. Landslide associated with the May 12, 2008 Wenchuan earthquake: Implications for the erosion and tectonic evolution of the Longmen Shan. Tectonophysics 491, 244–252.
Parker, R.N., Densmore, A.L., Rosser, N.J., de Michele, M., Li, Y., Huang, R., Whadcoat, S., Petley, D.N., 2011. Mass wasting triggered by the 2008 Wenchuan earthquake is greater than orogenic growth. Nature Geoscience 4, 449–452.
Pearce, A.J., Watson, A.J., 1986. Effects of earthquake-induced landslides on sediment budget and transport over a 50-yr period. Geology 14, 52–55.
Ran, Y., Chen, L., Chen, J., Wang, H., Chen, G., Yin, J., Shi, X., Li, C., Xu, X., 2010. Paleoseismic evidence and repeat time of large earthquakes at three sites along the Longmenshan fault zone. Tectonophysics 491, 141–153.
Shen, Z., Sun, J., Zhang, P., Wan, Y., Wang, M., Bürgmann, R., Zeng, Y., Gan, W., Liao, H., Wang, Q., 2009. Slip maxima at fault junctions and rupturing of barriers during the 2008 Wenchuan earthquake. Nature Geoscience 2, 718–724.
Stark, C.P., Hovius, N., 2001. The characterization of landslide size distributions. Geophysics Research Letters 28, 1091–1094.

Tang, C., Zhu, J., Li, W., Liang, J., 2009. Rainfall-triggered debris flow following the Wenchuan earthquake. Bulletin of Engineering Geology and the Environment 68, 187–194.

USGS, 2008. Magnitude 7.9 - Eastern Sichuan, China, 2008 May 12 06:28:01UTC. , http://earthquake.usgs.gov/earthquakes/eqinthenews/2008/us2008ryan/2008.

van den Eeckhaut, M., Poesen, J., Govers, G., Verstraeten, G., Demoulin, A., 2007. Characteristics of the size distribution of recent and historical landslides in a populated hilly region. Earth and Planetary Science Letters 256, 588–603.

van Westen, C.J., Castellanos, E., Kuriakose, S.L., 2008. Spatial data for landslide susceptibility, hazard, and vulnerability assessment: An overview. Engineering Geology 102, 112–131.

Walder, J.S., O'Connor, J.E., 1997. Methods for predicting peak discharge of floods caused by failure of natural and constructed earthen dams. Water Resources Research 33, 2337–2348.

Whipple, K.X., 2004. Bedrock rivers and the geomorphology of active orogens. Annual Reviews in Earth and Planetary Sciences 32, 151–185.

Xu, Q., Fan, X., Huang, R., van Westen, C.J., 2009a. Landslide dams triggered by the Wenchuan earthquake, Sichuan Province, south west China. Bulletin of Engineering Geology and the Environment 68, 373–386.

Xu, X., Wen, X., Yu, G., Chen, G., Klinger, Y., Hubbard, J., Shaw, J., 2009b. Coseismic reverse- and oblique-slip surface faulting generated by the 2008 M_w 7.9 Wenchuan earthquake, China. Geology 37, 515–518.

Yanites, B.J., Turker, G.E., Mueller, K.J., Chen, Y.G., 2010. How rivers react to large earthquakes: Evidence from central Taiwan. Geology 38, 639–642.

Zhang, X., 2010. Preliminary study on hydrological emergency monitoring scheme for dammed lakes. Automation in Water Recourses and Hydrology 1, 1–5 (in Chinese).

Please cite this article as: Fan, X., et al., Transient water and sediment storage of the decaying landslide dams induced by the 2008 Wenchuan earthquake, China, Geomorphology (2012), doi:10.1016/j.geomorph.2012.05.003